Keldysh Space Control of Charge Dynamics in a Strongly Driven Mott Insulator

Xinwei Li,[1,2,*] Honglie Ning,[1,2,*] Omar Mehio,[1,2,*] Hengdi Zhao,[3] Min-Cheol Lee,[4,5] Kyungwan Kim,[6] Fumihiko Nakamura,[7] Yoshiteru Maeno,[8] Gang Cao,[3] and David Hsieh[1,2,†]

[1]*Institute for Quantum Information and Matter, California Institute of Technology, Pasadena, California 91125, USA*
[2]*Department of Physics, California Institute of Technology, Pasadena, California 91125, USA*
[3]*Department of Physics, University of Colorado, Boulder, Colorado 80309, USA*
[4]*Center for Integrated Nanotechnologies, Los Alamos National Laboratory, Los Alamos, New Mexico 87545, USA*
[5]*Center for Correlated Electron Systems, Institute for Basic Science, Seoul 08826, Republic of Korea*
[6]*Department of Physics, Chungbuk National University, Cheongju, Chungbuk 28644, Republic of Korea*
[7]*Department of Education and Creation Engineering, Kurume Institute of Technology, Fukuoka 830-0052, Japan*
[8]*Department of Physics, Graduate School of Science, Kyoto University, Kyoto 606-8502, Japan*

(Received 24 October 2021; revised 20 February 2022; accepted 11 April 2022; published 6 May 2022)

The fate of a Mott insulator under strong low frequency optical driving conditions is a fundamental problem in quantum many-body dynamics. Using ultrafast broadband optical spectroscopy, we measured the transient electronic structure and charge dynamics of an off-resonantly pumped Mott insulator Ca_2RuO_4. We observe coherent bandwidth renormalization and nonlinear doublon-holon pair production occurring in rapid succession within a sub-100-fs pump pulse duration. By sweeping the electric field amplitude, we demonstrate continuous bandwidth tuning and a Keldysh crossover from a multiphoton absorption to quantum tunneling dominated pair production regime. Our results provide a procedure to control coherent and nonlinear heating processes in Mott insulators, facilitating the discovery of novel out-of-equilibrium phenomena in strongly correlated systems.

DOI: 10.1103/PhysRevLett.128.187402

The response of a Mott insulator to a strong electric field is a fundamental question in the study of nonequilibrium correlated many-body systems [1–15]. In the dc limit, a breakdown of the insulating state occurs when the field strength exceeds the threshold for producing pairs of doubly occupied (doublon) and empty (holon) sites by quantum tunneling, in analogy to the Schwinger mechanism for electron-positron pair production out of the vacuum [16]. Recently, the application of strong low frequency ac electric fields has emerged as a potential pathway to induce insulator-to-metal transitions [17–20], realize efficient high-harmonic generation [21,22], and coherently manipulate band structure and magnetic exchange interactions in Mott insulators [23–28]. Therefore there is growing interest to understand doublon-holon (d-h) pair production and their nonthermal dynamics in the strong field ac regime.

Strong ac field induced d-h pair production has been theoretically studied using Landau-Dykhne adiabatic perturbation theory [29] along with a suite of nonequilibrium numerical techniques [17,21,22,29–32]. Notably, d-h pairs are primarily produced through two nonlinear mechanisms: multiphoton absorption and quantum tunneling [29,33]. The two regimes are characterized by distinct electric field scaling laws and momentum space distributions of d-h pairs. By tuning the Keldysh adiabaticity parameter $\gamma_K = \hbar\omega_{\mathrm{pump}}/(eE_{\mathrm{pump}}\xi)$ through unity, where ω_{pump} is the pump frequency, E_{pump} is the pump electric field, e is electron charge, and ξ is the d-h correlation length, a crossover from a multiphoton dominated ($\gamma_K > 1$) to a tunneling dominated ($\gamma_K < 1$) regime can in principle be induced. However, direct experimental tests are lacking owing to the challenging need to combine strong tunable low frequency pumping fields with sensitive ultrafast probes of nonequilibrium distribution functions.

We devise a protocol to study these predicted phenomena using ultrafast broadband optical spectroscopy. As a test bed, we selected the multiband Mott insulator Ca_2RuO_4. Below a metal-to-insulator transition temperature $T_{\mathrm{MIT}} = 357$ K, a Mott gap ($\Delta = 0.6$ eV) opens within its 2/3-filled Ru $4d$ t_{2g} manifold [34–37], with a concomitant distortion of the lattice [38]. Upon further cooling, the material undergoes an antiferromagnetic transition at $T_N = 113$ K into a Néel ordered state. It has recently been shown that for temperatures below T_{MIT}, reentry into a metallic phase can be induced by a remarkably weak dc electric field of order 100 V/cm [39], making Ca_2RuO_4 a promising candidate for exhibiting efficient nonlinear pair production.

To estimate the response of Ca_2RuO_4 to a low frequency ac electric field, we calculated the d-h pair production rate (Γ) over the Keldysh parameter space using a Landau-Dykhne method developed by Oka [29]. Experimentally determined values of the Hubbard model parameters for Ca_2RuO_4 were used as inputs [40]. As shown in Fig. 1(a), Γ is a generally increasing function of E_{pump} and $\hbar\omega_{\mathrm{pump}}$. For a

 © 2022 American Physical Society

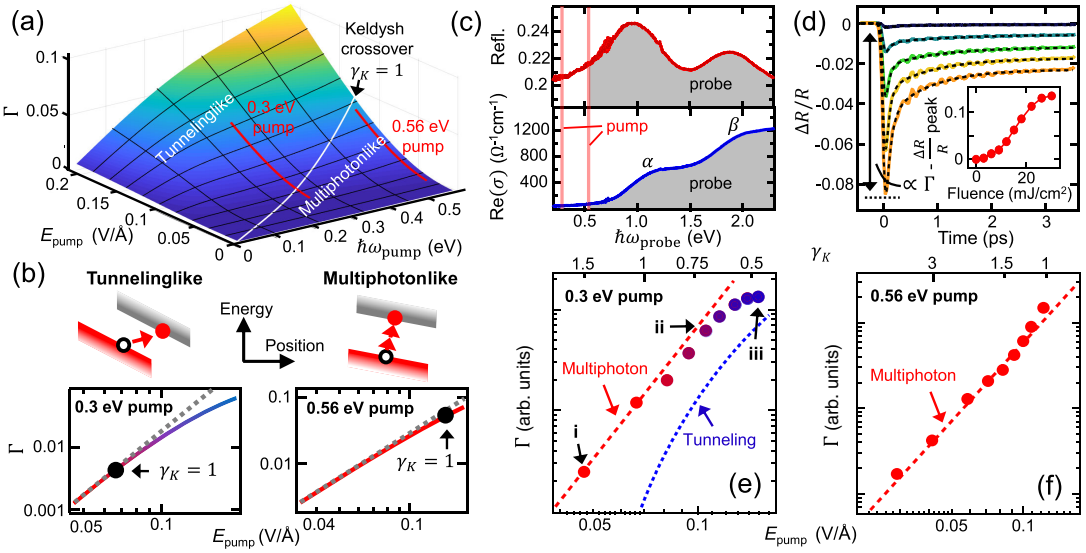

FIG. 1. Resolving Keldysh tuning using pump-probe spectroscopy. (a) Γ calculated across Keldysh space using the Landau-Dykhne method. (b) Constant energy cuts along the red lines shown in (a) plotted on a logarithmic scale. Black dots mark the Keldysh crossover. Gray dashed lines show the scaling relation in the multiphoton regime. Schematics of the multiphoton and tunneling processes are shown above. (c) Equilibrium reflectivity (top) and conductivity (bottom) spectra of Ca_2RuO_4 at 20 K. The 0.3 and 0.56 eV pump energies are marked by vertical red lines. The probe energy range is shaded gray. (d) Select 0.3 eV pump 1.77 eV probe $\Delta R/R$ traces at fluences of 3, 9, 15, 22, and 30 mJ/cm^2 (top to bottom). Dashed lines are fits detailed in Ref. [40]. Inset: peak $\Delta R/R$ versus fluence showing nonlinearity. (e),(f) Experimental cuts through the same regions of parameter space as in (b). Error bars are smaller than data markers. Scaling relations for multiphoton and tunneling behavior are overlaid as red and blue dashed lines, respectively.

fixed ω_{pump}, the predicted scaling of Γ with E_{pump} is clearly different on either side of the Keldysh crossover line ($\gamma_K = 1$), evolving from power law behavior $\Gamma \propto (E_{pump})^a$ in the multiphoton regime to threshold behavior $\Gamma \propto \exp(-b/E_{pump})$ in the tunneling regime [Fig. 1(b)].

At time delays where coherent nonlinear processes are absent, the transient pump-induced change in reflectivity of a general gapped material is proportional to the density of photoexcited quasiparticles [51–53], which, upon dividing by a constant pump pulse duration (~100 fs), yields Γ. Differential reflectivity ($\Delta R/R$) transients from Ca_2RuO_4 single crystals were measured at $T = 80$ K using several different subgap pump photon energies ($\hbar\omega_{pump} < \Delta$) in the midinfrared region, and across an extensive range of probe photon energies ($\hbar\omega_{probe}$) in the near-infrared region spanning both the α and β absorption peaks [Fig. 1(c)]. These two band edge features can be assigned to optical transitions within the Ru t_{2g} manifold [37,54]. Figure 1(d) shows reflectivity transients at various fluences measured using $\hbar\omega_{pump} = 0.3$ eV and $\hbar\omega_{probe} = 1.77$ eV. Upon pump excitation, we observe a rapid resolution-limited drop in $\Delta R/R$. With increasing fluence, the minimum value of $\Delta R/R$ becomes larger, indicating a higher value of Γ within the pump pulse duration. This is followed by exponential recovery as the d-h pairs thermalize and recombine [40]. By plotting Γ against the peak value of E_{pump} (measured in vacuum), we observe a change from power law scaling to threshold behavior when $E_{pump} > 0.07$ V/Å [Fig. 1(e)], in remarkable agreement with our calculated Keldysh crossover [Figs. 1(a) and 1(b)]. In contrast, measurements performed using 0.56 eV pumping exhibit exclusively power law scaling over the same E_{pump} range [Fig. 1(f)], again consistent with our model.

A predicted hallmark of the Keldysh crossover is a change in width of the nonthermal distribution of d-h pairs in momentum space [29]. In the multiphoton regime, doublons and holons primarily occupy the conduction and valence band edges, respectively, resulting in a pair distribution function (P_p) sharply peaked about zero momentum ($p = 0$). In the tunneling regime, the peak drastically broadens, reflecting the increased spatial localization of d-h pairs. Using the Landau-Dykhne method [40], we calculated the evolution of P_p for Ca_2RuO_4 as a function of E_{pump} through the Keldysh crossover. Figure 2(a) displays P_p curves at three successively larger E_{pump} values corresponding to (i) $\gamma_K = 1.49$, (ii) $\gamma_K = 0.75$, and (iii) $\gamma_K = 0.47$, which show a clearly broadening width along with increasing amplitude.

To demonstrate how signatures of a changing P_p width are borne out in experiments, we simulate the effects of different nonthermal electronic distribution functions on the broadband optical response of a model insulator. Assuming a direct-gap quasi-two-dimensional insulator with cosine band dispersion in the momentum plane (p_x, p_y), the optical susceptibility computed using the density matrix formalism can be expressed as [40,55]

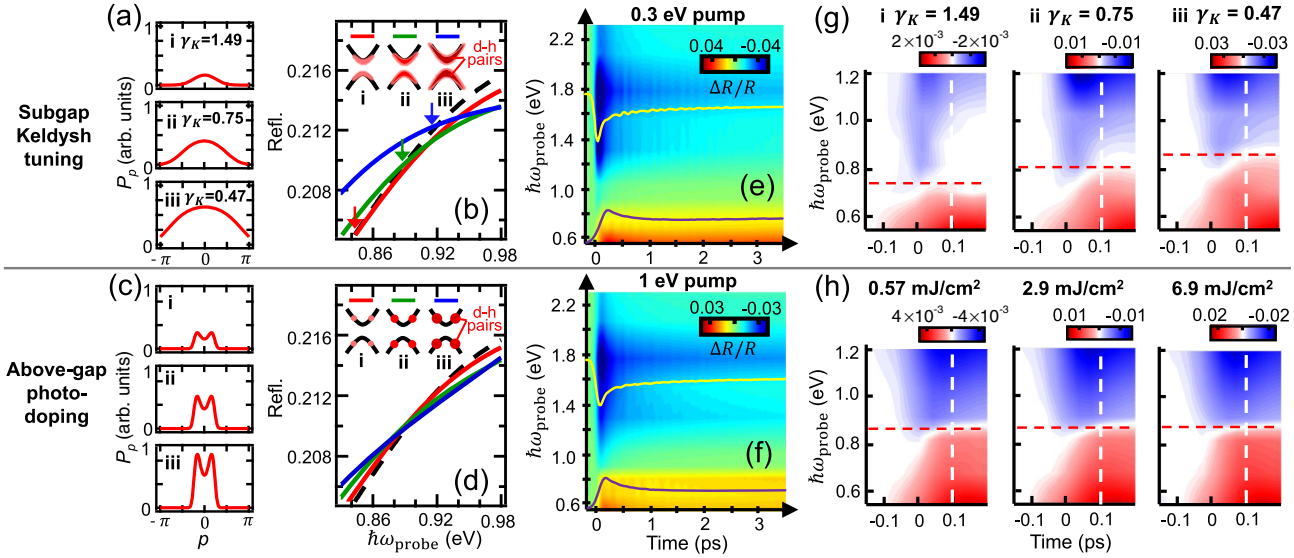

FIG. 2. Nonthermal pair distribution through the Keldysh crossover. (a) Calculated P_p for conditions (i)–(iii) using the Landau-Dykhne method. (b) Simulated nonequilibrium reflectivity spectra for subgap pumping. (c),(d) Analogs of (a) and (b) but simulated for above-gap pumping. Fluence increases from (i) to (iii). Black curves in (b) and (d) are the equilibrium spectra. Arrows in (b) mark the crossing points between the nonequilibrium and equilibrium curves. Experimental $\Delta R/R$ maps of Ca_2RuO_4 for (e) 0.3 eV pump (fluence 30 mJ/cm^2) and (f) 1 eV pump (fluence 7 mJ/cm^2). Two representative constant energy cuts (yellow, 1.77 eV; purple, 0.56 eV) are overlaid. (g) Enlargement of $\Delta R/R$ maps for 0.3 eV pump using three pump fluences [marked in Fig. 1(e)] corresponding to conditions (i)–(iii) in (a). (h) Enlargement of $\Delta R/R$ maps for 1 eV pump using three pump fluences indicated above. White dashed lines mark $t = 0.1$ ps. Red dashed lines are guides to the eye for the $\hbar\omega_{probe}$ where $\Delta R/R$ changes sign at $t = 0.1$ ps.

$$\chi = \sum_{p_x,p_y} C\mathcal{L}[\hbar\omega_{probe} - \Delta(p_x,p_y)][N_v(p_x,p_y) - N_c(p_x,p_y)],$$

where C is a constant incorporating the transition matrix element, $\mathcal{L}$ represents a Lorentzian oscillator centered at the gap energy $\Delta(p_x, p_y)$, and N_v and N_c are the occupations of the valence and conduction bands, respectively. As will be shown later [Fig. 3(a)], it is valid to assume that $\Delta(p_x, p_y)$ decreases in proportion to the number of excitations [40]. Figure 2(b) shows simulated reflectivity spectra around the band edge—converted from χ via the Fresnel equations—using Gaussian functions for N_v and N_c of variable width to approximate the P_p line shapes [Fig. 2(a)] [40]. As P_p evolves from condition (i) to (iii), we find that the intersection between the nonequilibrium and equilibrium reflectivity spectra shifts to progressively higher energy. For comparison, we also performed simulations under resonant photodoping conditions using the direct-gap insulator model. Figure 2(c) displays three P_p curves at successively larger E_{pump} values, which were chosen such that the total number of excitations match those in Fig. 2(a). Each curve exhibits maxima at nonzero momenta where $\hbar\omega_{pump} = \Delta(|p|)$ is satisfied. In stark contrast to the subgap pumping case, the amplitude of P_p increases with E_{pump} but the width remains unchanged. This results in the nonequilibrium reflectivity spectra all intersecting the equilibrium spectrum at the same energy, forming an isosbestic point [Fig. 2(d)]. The presence or absence of an isosbestic point is therefore a key distinguishing feature between Keldysh space tuning and photodoping. This criterion can be derived from a more general analytical model [40], which shows that a key condition for identifying a Keldysh crossover is that $\Delta R/R$ spectra at difference fluences do not scale.

Probe photon energy-resolved $\Delta R/R$ maps of Ca_2RuO_4 were measured in both the Keldysh tuning ($\hbar\omega_{pump} = 0.3$ eV) and photodoping ($\hbar\omega_{pump} = 1$ eV) regimes. As shown in Figs. 2(e) and 2(f), the extremum in $\Delta R/R$, denoting the peak d-h density, occurs near a time $t = 0.1$ ps measured with respect to when the pump and probe pulses are exactly overlapped ($t = 0$). This is followed by a rapid thermalization of d-h pairs as indicated by the fast exponential relaxation in $\Delta R/R$, which will be discussed later [40]. Figure 2(g) shows $\Delta R/R$ maps acquired in the subgap pumping regime for three different pump fluences corresponding to conditions (i)–(iii) in Figs. 1(e) and 2(a). Focusing on the narrow time window around $t = 0.1$ ps, where the d-h distribution is highly nonthermal, we observe that $\Delta R/R$ changes sign across a well-defined probe energy (dashed red line), marking a crossing point of the transient and equilibrium reflectivity spectra. As γ_K decreases, the crossing energy increases, evidencing an absence of an isosbestic point. Analogous maps acquired in the photodoping regime [Fig. 2(h)] also exhibit a sign change. However, the crossing energy remains constant over an order of magnitude change in fluence, consistent with an

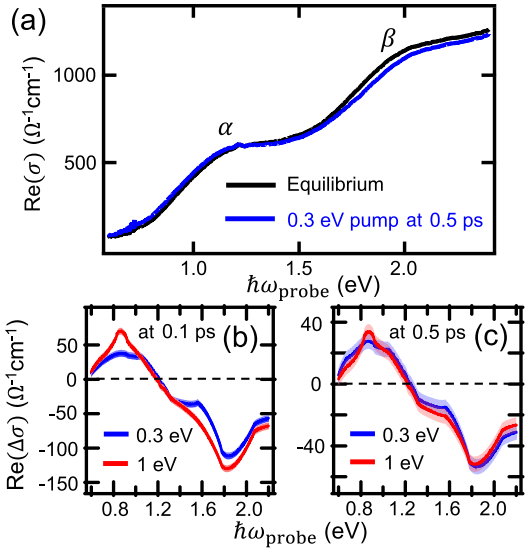

FIG. 3. Nonequilibrium conductivity transients. (a) Conductivity spectra of Ca_2RuO_4 in the unpumped equilibrium state at 80 K and the 0.3 eV pumped nonequilibrium state at $t = 0.5$ ps (fluence 26 mJ/cm^2). (b) Comparison of differential conductivity spectra between 0.3 eV pump ($\Delta\sigma_{0.3\ \mathrm{eV}}$) and scaled 1 eV pump ($A\Delta\sigma_{1\ \mathrm{eV}}$) cases at $t = 0.1$ ps and (c) $t = 0.5$ ps. Red and blue shades indicate error estimated from the ω_{probe}-dependent fluctuations of the experimental $\Delta\sigma$ spectra.

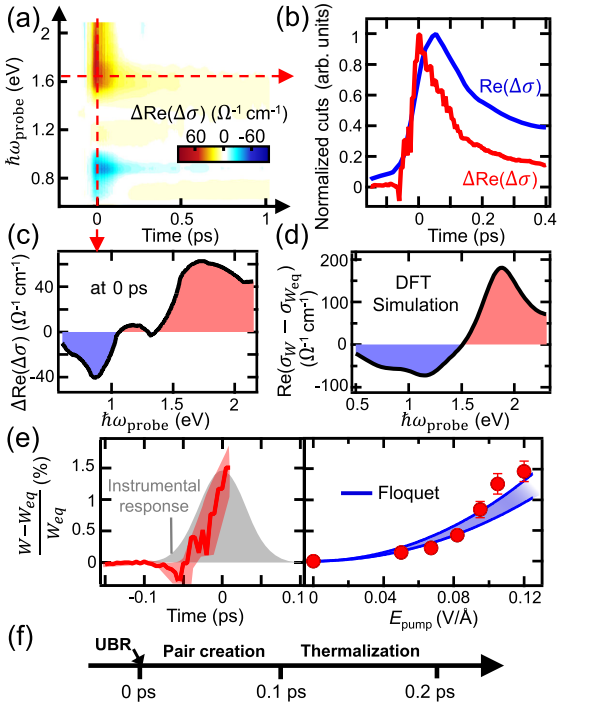

FIG. 4. Ultrafast coherent bandwidth renormalization. (a) $\Delta(\Delta\sigma)$ map obtained by subtracting scaled $\Delta\sigma_{1\ \mathrm{eV}}$ from $\Delta\sigma_{0.3\ \mathrm{eV}}$ spectra. (b) A constant probe energy cut at 1.65 eV [dashed horizontal line in (a)] plotted together with $\Delta\sigma_{0.3\ \mathrm{eV}}$. (c) A constant time cut at $t = 0$ [dashed vertical line in (a)]. (d) DFT simulation of the spectrum change induced by bandwidth broadening. σ_W ($\sigma_{W_{\mathrm{eq}}}$) is conductivity with (without) bandwidth broadening. (e) (left) Quantitative extraction of pump-induced bandwidth modification versus t (with $E_{\mathrm{pump}} = 0.12$ V/Å) and (right) versus E_{pump} (with $t = 0$ ps) based on fitting to DFT calculations. Red shaded region: error bar. Blue shaded region: Floquet theory prediction based on a periodically driven two-site cluster Hubbard model. Upper and lower bounds assume $U = 3$ eV [37] and $U = 3.5$ eV [34], respectively, where U is the on-site Coulomb energy, with no other adjustable parameters. (f) Chronology of nonthermal processes following an impulsive subgap drive.

isosbestic point. These measurements corroborate our simulations and highlight the unique distribution control afforded by Keldysh tuning.

To study the d-h thermalization dynamics in more detail, we used a Kramers-Kronig transformation to convert our differential reflectivity spectra into differential conductivity ($\Delta\sigma$) spectra [40]. Figure 3(a) shows the real part of the transient conductivity measured in the thermalized state ($t = 0.5$ ps) following an 0.3 eV pump pulse of fluence 26 mJ/cm^2 ($\gamma_K = 0.5$), overlaid with the equilibrium conductivity. Subgap pumping induces a spectral weight transfer from the β to α peak and a slight redshift of the band edge, likely due to free carrier screening of the Coulomb interactions [56]. Unlike in the dc limit, there is no sign of Mott gap collapse despite E_{pump} exceeding 10^9 V/m. To verify that the electronic subsystem indeed thermalizes by $t = 0.5$ ps, we compare the real parts of $\Delta\sigma_{0.3\ \mathrm{eV}}$ (fluence 26 mJ/cm^2) and $\Delta\sigma_{1\mathrm{eV}}$ (fluence 4 mJ/cm^2), the change in conductivity induced by subgap and above-gap pumping, respectively, at both $t = 0.1$ and 0.5 ps. A scaling factor A is applied to $\Delta\sigma_{1\ \mathrm{eV}}$ to account for any differences in excitation density. As shown in Fig. 3(b), the $t = 0.1$ ps curves do not agree within any scale factor. This is expected because the linear and nonlinear pair production processes initially give rise to very different nonthermal distributions (Fig. 2). Conversely, by $t = 0.5$ ps, the curves overlap very well [Fig. 3(c)], indicating that the system has lost memory of how the d-h pairs were produced and is thus completely thermalized.

Based on the observations in Figs. 3(b) and 3(c), the nonthermal window can be directly resolved by evaluating the time interval over which the quantity $\Delta(\Delta\sigma) = \Delta\sigma_{0.3\ \mathrm{eV}} - A \times \Delta\sigma_{1\ \mathrm{eV}}$ is nonzero [40]. Figure 4(a) shows the complete temporal mapping of $\Delta(\Delta\sigma)$ spectra. The signal is finite only around $t = 0$ ps and is close to zero otherwise, supporting the validity our subtraction protocol. By taking a constant energy cut, we can extract a thermalization time constant of around 0.2 ps [Fig. 4(b)]. Interestingly, $\Delta R/R$ and $\Delta\sigma_{0.3\ \mathrm{eV}}$, which both track the d-h pair density, peak near 0.1 ps, whereas $\Delta(\Delta\sigma)$ peaks earlier at $t = 0$ when the d-h pair density is still quite low. This implies the existence of an additional coherent

nonthermal process that scales with E_{pump}, which peaks at $t = 0$, rather than with the *d*-*h* density.

To identify the physical process responsible for the $t = 0$ signal, we examined how the electronic structure of Ca_2RuO_4 would need to change in order to produce the $\Delta(\Delta\sigma)$ profile observed at $t = 0$ [Fig. 4(c)]. Using density functional theory (DFT), we performed an *ab initio* calculation of the optical conductivity of Ca_2RuO_4 based on its reported lattice and magnetic structures below T_N. The tilt angle of the RuO_6 octahedra was then systematically varied in our calculation as a means to simulate a changing electronic bandwidth [40]. We find that both the real and imaginary parts of the measured $\Delta(\Delta\sigma)$ spectrum at $t = 0$ are reasonably well reproduced by our calculations if we assume the bandwidth of the driven system (W) to exceed that in equilibrium W_{eq} [Fig. 4(d)] [40]. This points to the coherent nonthermal process being a unidirectional ultrafast bandwidth renormalization (UBR) process that predominantly occurs under subgap pumping conditions [Fig. 4(f)].

Coherent UBR can in principle occur via photoassisted virtual hopping between lattice sites, which has recently been proposed as a pathway to dynamically engineer the electronic and magnetic properties of Mott insulators [23–28]. To quantitatively extract the time and E_{pump} dependence of the fractional bandwidth change $(W - W_{\mathrm{eq}})/W_{\mathrm{eq}}$, we collected $\Delta(\Delta\sigma)$ spectra as a function of both time delay and pump fluence and fit them to DFT simulations [40]. As shown in Fig. 4(e), the bandwidth change exhibits a pulse-width limited rise with a maximum $t = 0$ value that increases monotonically with the peak pump field, reaching up to a relatively large amplitude of 1.5% at $E_{\mathrm{pump}} = 0.12\ \mathrm{V/\AA}$, comparable to the bandwidth increases induced by doping [36] and pressure [57]. Independently, we also calculated the field dependence of $(W - W_{\mathrm{eq}})/W_{\mathrm{eq}}$ expected from photoassisted virtual hopping by solving a periodically driven two-site Hubbard model in the Floquet formalism [23,40], using the same model parameters for Ca_2RuO_4 as in our Landau-Dykhne calculations [Fig. 1(a)]. We find a remarkable match to the data without any adjustable parameters [Fig. 4(e)]. Since bandwidth renormalization increases with the Floquet parameter $(eaE_{\mathrm{pump}})/\hbar\omega_{\mathrm{pump}}$ in the case of photoassisted virtual hopping, where a is the intersite distance, this naturally explains why subgap pumping induces the much larger UBR effect compared to above-gap pumping.

The ability to rationally tune a Mott insulator *in situ* over Keldysh space enables targeted searches for exotic out-of-equilibrium phenomena such as strong correlation assisted high-harmonic generation [21,22], coherent dressing of quasiparticles [58], Wannier-Stark localization [2,17], ac dielectric breakdown [29], and dynamical Franz-Keldysh effects [32,59], which are predicted to manifest in separate regions of Keldysh space. It also provides control over the nonlinear *d*-*h* pair production rate—the primary source of heating and decoherence under subgap pumping conditions—in Mott systems, which is crucial for experimentally realizing coherent Floquet engineering of strongly correlated electronic phases.

We thank Swati Chaudhary, Nicolas Tancogne-Dejean, and Tae Won Noh for useful discussions. The first-principles calculations in this work were performed using the QUANTUM ESPRESSO package. Time-resolved spectroscopic measurements were supported by the Institute for Quantum Information and Matter (IQIM), a NSF Physics Frontiers Center (PHY-1733907). D. H. also acknowledges support for instrumentation from the David and Lucile Packard Foundation and from ARO MURI Grant No. W911NF-16-1-0361. X. L. acknowledges support from the Caltech Postdoctoral Prize Fellowship and the IQIM. G. C. acknowledges NSF support via Grant No. DMR 1903888. M.-C. L. acknowledges funding supports from the Research Center Program of IBS (Institute for Basic Science) in Korea (IBS-R009-D1). K. K. was supported by the National Research Foundation of Korea (NRF) grant funded by the Korea government (MSIT) (No. 2020R1A2C3013454). Y. M. was supported by the JSPS Core-to-Core Program No. JPJSCCA20170002 as well as the JSPS Kakenhi No. JP17H06136.

*These authors contributed equally to this work.
†dhsieh@caltech.edu

[1] M. Eckstein, T. Oka, and P. Werner, Phys. Rev. Lett. **105**, 146404 (2010).
[2] W.-R. Lee and K. Park, Phys. Rev. B **89**, 205126 (2014).
[3] Z. Lenarčič and P. Prelovšek, Phys. Rev. Lett. **108**, 196401 (2012).
[4] J. Li, C. Aron, G. Kotliar, and J. E. Han, Phys. Rev. Lett. **114**, 226403 (2015).
[5] T. Oka and H. Aoki, Phys. Rev. Lett. **95**, 137601 (2005).
[6] P. Diener, E. Janod, B. Corraze, M. Querré, C. Adda, M. Guilloux-Viry, S. Cordier, A. Camjayi, M. Rozenberg, M. P. Besland, and L. Cario, Phys. Rev. Lett. **121**, 016601 (2018).
[7] A. Asamitsu, Y. Tomioka, H. Kuwahara, and Y. Tokura, Nature (London) **388**, 50 (1997).
[8] H. Chu *et al.*, Nat. Commun. **11**, 1793 (2020).
[9] S. Wall, D. Brida, S. R. Clark, H. P. Ehrke, D. Jaksch, A. Ardavan, S. Bonora, H. Uemura, Y. Takahashi, T. Hasegawa, H. Okamoto, G. Cerullo, and A. Cavalleri, Nat. Phys. **7**, 114 (2011).
[10] H. Okamoto, H. Matsuzaki, T. Wakabayashi, Y. Takahashi, and T. Hasegawa, Phys. Rev. Lett. **98**, 037401 (2007).
[11] M. Mitrano, G. Cotugno, S. R. Clark, R. Singla, S. Kaiser, J. Stähler, R. Beyer, M. Dressel, L. Baldassarre, D. Nicoletti, A. Perucchi, T. Hasegawa, H. Okamoto, D. Jaksch, and A. Cavalleri, Phys. Rev. Lett. **112**, 117801 (2014).
[12] N. Strohmaier, D. Greif, R. Jördens, L. Tarruell, H. Moritz, T. Esslinger, R. Sensarma, D. Pekker, E. Altman, and E. Demler, Phys. Rev. Lett. **104**, 080401 (2010).

[13] Z. Lenarčič and P. Prelovšek, Phys. Rev. Lett. **111**, 016401 (2013).
[14] R. Sensarma, D. Pekker, E. Altman, E. Demler, N. Strohmaier, D. Greif, R. Jördens, L. Tarruell, H. Moritz, and T. Esslinger, Phys. Rev. B **82**, 224302 (2010).
[15] M. Eckstein and P. Werner, Phys. Rev. B **84**, 035122 (2011).
[16] J. Schwinger, Phys. Rev. **82**, 664 (1951).
[17] Y. Murakami and P. Werner, Phys. Rev. B **98**, 075102 (2018).
[18] F. Giorgianni, J. Sakai, and S. Lupi, Nat. Commun. **10**, 1159 (2019).
[19] B. Mayer, C. Schmidt, A. Grupp, J. Bühler, J. Oelmann, R. E. Marvel, R. F. Haglund, T. Oka, D. Brida, A. Leitenstorfer, and A. Pashkin, Phys. Rev. B **91**, 235113 (2015).
[20] H. Yamakawa, T. Miyamoto, T. Morimoto, T. Terashige, H. Yada, N. Kida, M. Suda, H. Yamamoto, R. Kato, K. Miyagawa, K. Kanoda, and H. Okamoto, Nat. Mater. **16**, 1100 (2017).
[21] S. Imai, A. Ono, and S. Ishihara, Phys. Rev. Lett. **124**, 157404 (2020).
[22] R. E. F. Silva, I. V. Blinov, A. N. Rubtsov, O. Smirnova, and M. Ivanov, Nat. Photonics **12**, 266 (2018).
[23] J. H. Mentink, K. Balzer, and M. Eckstein, Nat. Commun. **6**, 6708 (2015).
[24] K. Hejazi, J. Liu, and L. Balents, Phys. Rev. B **99**, 205111 (2019).
[25] R. V. Mikhaylovskiy, E. Hendry, A. Secchi, J. H. Mentink, M. Eckstein, A. Wu, R. V. Pisarev, V. V. Kruglyak, M. I. Katsnelson, T. Rasing, and A. V. Kimel, Nat. Commun. **6**, 8190 (2015).
[26] G. Batignani, D. Bossini, N. Di Palo, C. Ferrante, E. Pontecorvo, G. Cerullo, A. Kimel, and T. Scopigno, Nat. Photonics **9**, 506 (2015).
[27] M. Claassen, H.-C. Jiang, B. Moritz, and T. P. Devereaux, Nat. Commun. **8**, 1192 (2017).
[28] Y. Wang, T. P. Devereaux, and C.-C. Chen, Phys. Rev. B **98**, 245106 (2018).
[29] T. Oka, Phys. Rev. B **86**, 075148 (2012).
[30] N. Tsuji, T. Oka, P. Werner, and H. Aoki, Phys. Rev. Lett. **106**, 236401 (2011).
[31] A. Takahashi, H. Itoh, and M. Aihara, Phys. Rev. B **77**, 205105 (2008).
[32] N. Tancogne-Dejean, M. A. Sentef, and A. Rubio, Phys. Rev. B **102**, 115106 (2020).
[33] S. Y. Kruchinin, F. Krausz, and V. S. Yakovlev, Rev. Mod. Phys. **90**, 021002 (2018).
[34] E. Gorelov, M. Karolak, T. O. Wehling, F. Lechermann, A. I. Lichtenstein, and E. Pavarini, Phys. Rev. Lett. **104**, 226401 (2010).
[35] Q. Han and A. Millis, Phys. Rev. Lett. **121**, 067601 (2018).
[36] Z. Fang, N. Nagaosa, and K. Terakura, Phys. Rev. B **69**, 045116 (2004).
[37] J. H. Jung, Z. Fang, J. P. He, Y. Kaneko, Y. Okimoto, and Y. Tokura, Phys. Rev. Lett. **91**, 056403 (2003).
[38] M. Braden, G. André, S. Nakatsuji, and Y. Maeno, Phys. Rev. B **58**, 847 (1998).
[39] F. Nakamura, M. Sakaki, Y. Yamanaka, S. Tamaru, T. Suzuki, and Y. Maeno, Sci. Rep. **3**, 2536 (2013).
[40] See Supplemental Material at http://link.aps.org/supplemental/10.1103/PhysRevLett.128.187402 for extensive simulation and experimental details, which includes Refs. [41–50].
[41] G. Cao, S. McCall, V. Dobrosavljevic, C. S. Alexander, J. E. Crow, and R. P. Guertin, Phys. Rev. B **61**, R5053 (2000).
[42] T. F. Qi, O. B. Korneta, S. Parkin, J. Hu, and G. Cao, Phys. Rev. B **85**, 165143 (2012).
[43] M.-C. Lee, C. H. Kim, I. Kwak, J. Kim, S. Yoon, B. C. Park, B. Lee, F. Nakamura, C. Sow, Y. Maeno, T. W. Noh, and K. W. Kim, Phys. Rev. B **98**, 161115(R) (2018).
[44] C. A. Stafford and A. J. Millis, Phys. Rev. B **48**, 1409 (1993).
[45] D. M. Roessler, Br. J. Appl. Phys. **16**, 1119 (1965).
[46] A. Eschenmoser and C. Wintner, Science **196**, 1410 (1977).
[47] L. M. Woods, Phys. Rev. B **62**, 7833 (2000).
[48] J. Bertinshaw, N. Gurung, P. Jorba, H. Liu, M. Schmid, D. T. Mantadakis, M. Daghofer, M. Krautloher, A. Jain, G. H. Ryu, O. Fabelo, P. Hansmann, G. Khaliullin, C. Pfleiderer, B. Keimer, and B. J. Kim, Phys. Rev. Lett. **123**, 137204 (2019).
[49] M.-C. Lee, C. H. Kim, I. Kwak, C. W. Seo, C. Sohn, F. Nakamura, C. Sow, Y. Maeno, E.-A. Kim, T. W. Noh, and K. W. Kim, Phys. Rev. B **99**, 144306 (2019).
[50] N. Tancogne-Dejean, M. A. Sentef, and A. Rubio, Phys. Rev. Lett. **121**, 097402 (2018).
[51] N. Gedik, P. Blake, R. C. Spitzer, J. Orenstein, R. Liang, D. A. Bonn, and W. N. Hardy, Phys. Rev. B **70**, 014504 (2004).
[52] E. E. M. Chia, J.-X. Zhu, H. J. Lee, N. Hur, N. O. Moreno, E. D. Bauer, T. Durakiewicz, R. D. Averitt, J. L. Sarrao, and A. J. Taylor, Phys. Rev. B **74**, 140409(R) (2006).
[53] J. Demsar, K. Biljaković, and D. Mihailovic, Phys. Rev. Lett. **83**, 800 (1999).
[54] L. Das *et al.*, Phys. Rev. X **8**, 011048 (2018).
[55] E. Rosencher and B. Vinter, in *Optoelectronics*, edited by P. G. Piva (Cambridge University Press, Cambridge, England, 2002).
[56] D. Golež, M. Eckstein, and P. Werner, Phys. Rev. B **92**, 195123 (2015).
[57] F. Nakamura, T. Goko, M. Ito, T. Fujita, S. Nakatsuji, H. Fukazawa, Y. Maeno, P. Alireza, D. Forsythe, and S. R. Julian, Phys. Rev. B **65**, 220402(R) (2002).
[58] F. Novelli, G. De Filippis, V. Cataudella, M. Esposito, I. Vergara, F. Cilento, E. Sindici, A. Amaricci, C. Giannetti, D. Prabhakaran, S. Wall, A. Perucchi, S. Dal Conte, G. Cerullo, M. Capone, A. Mishchenko, M. Grüninger, N. Nagaosa, F. Parmigiani, and D. Fausti, Nat. Commun. **5**, 5112 (2014).
[59] A. Srivastava, R. Srivastava, J. Wang, and J. Kono, Phys. Rev. Lett. **93**, 157401 (2004).